Biomedical Signal Processing and Control 75 (2022) 103632

Contents lists available at ScienceDirect

Biomedical Signal Processing and Control

journal homepage: www.elsevier.com/locate/bspc

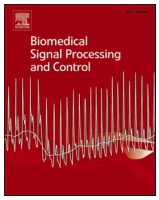

PPGMotion: Model-based detection of motion artifacts in photoplethysmography signals

Akash Kumar Maity *, Ashok Veeraraghavan, Ashutosh Sabharwal

Department of Electrical and Computer Engineering, Rice University, Houston, TX 77005, United States

ARTICLE INFO

Keywords:
Photoplethysmography
Motion artifacts
Morphology

ABSTRACT

Photoplethysmography (PPG) is used widely in health wearables to monitor biomarkers like heart rate. However, motion activities degrade the quality of the measured PPG signal, thereby reducing the accuracy of heart-rate estimation. Existing state-of-the-art methods for motion detection rely on the semi-periodic structure of PPG to detect the aperiodic motion artifacts, thereby failing in scenarios when motion contamination tends to be periodic. We propose a novel technique, PPGMotion, for detecting all types of motion artifacts in PPG signals with high accuracy, without the need for any reference motion signals. Our approach relies on the morphological structure of the artifact-free PPG signal. We compare our method against some classical methods on one synthetic and four real datasets – dataset (1) and (2) are obtained from finger pulse-oximeter under motion activities, dataset (3) and (4) are obtained from a wearable smartwatch. We show that for the synthetic dataset, the performance of PPGMotion is significantly better than existing work as the contaminated PPG tends to become periodic, with an increase in sensitivity of at least 20% over state-of-the-art methods. For real data, PPGMotion achieves similar performance for random motion artifact detection as the classical methods but performs significantly better when motion tends to be periodic, with at least 10% increase in sensitivity in detecting motion artifacts in datasets (2), (3), and (4).

1. Introduction

Continuous vital signs monitoring has been explored extensively in the past decade to improve ambulatory care, leading to better utilization of healthcare resources. Vital signs monitoring is feasible with photoplethysmography, commonly known as PPG, a non-invasive, optical technique for measuring blood volume change in arteries and microvasculature. The basic principle relies on light traversing the tissue with vasculature, with a sensor collecting light on the other end. The modulated light is detected and converted into a signal called the PPG signal, which reflects the blood volume change in synchrony with the cardiac cycle. A pulse oximeter, which uses PPG, has been long used for estimating oxygenation levels in clinical environments. Further research has shown that several other clinically relevant parameters related to cardiovascular health like Heart Rate Variability [1], Breathing Rate [2], and arterial stiffness [3] can be estimated from PPG signals.

In most cases, the sensor measurements either from a clinical-grade pulse-oximeter or a smartwatch are contaminated with noise. In a typical PPG measurement, there are two significant sources of noise - sensor noise and motion artifacts, which mainly arise from body movements while performing daily tasks or while performing physical exercise. In many cases, motion artifacts, when present, dominate as the primary source of the noise. The presence of motion artifacts in the PPG signal degrades the estimation of any clinically relevant parameters.

1.1. Prior literature

As a first step towards getting rid of any unwanted interference, one of the most common approaches taken is to filter the PPG signal within some frequency range in the heart rate bandwidth [4]. In [5], the authors demonstrated that the Chebyshev II filter was found to be the most effective among other filters in improving the quality of PPG signals. However, in many scenarios, the motion artifact spectrum overlaps in the heart rate bandwidth [6], thereby making it more challenging to separate out motion artifacts. Special types of filters, like the adaptive filters, have been proposed to cancel out the motion artifacts in the signal [7,8] using a reference motion signal. The reference motion signal is often obtained from additional hardware, say, an accelerometer. In [9], the authors have developed a framework in conjunction with a neural network that uses accelerometer signals to reduce the effects of

* Corresponding author.

https://doi.org/10.1016/j.bspc.2022.103632
Received 26 September 2021; Received in revised form 20 February 2022; Accepted 5 March 2022
Available online 13 March 2022
1746-8094/© 2022 Elsevier Ltd. All rights reserved.

motion on PPG signal measurements. In [10], the accelerometer signals are used with the motion-corrputed PPG signals to provide a robust estimate of heart-rate during intense physical exercise. However, accelerometer signals may not be accessible in some scenarios. Additionally, it has been noted in [11,12] that there might be no direct correlation between movements reflected in accelerometer data and motion artifacts in PPG signals. Moreover, the adaptive filters also operate on the clean section of the PPG signals, thereby introducing some distortions. It has also been reported that the reconstructed signal using these algorithms introduces some delay in the waveform, thus resulting in false interpretation [13].

Considering the above-mentioned factors, a simpler strategy is to aim for detecting the presence of motion corruption. The basic idea behind these approaches is that the clean PPG signal has a distinct quasi-periodic structure, and this structure is entirely violated in a motion corrupted segment [14,15]. A common approach is, therefore, to segment individual beats within a PPG signal recording and analyzing features of individual beats to distinguish the motion corrupted beats from the clean PPG counterparts [15]. Still, the performance of such techniques largely relies on the accuracy of PPG beat segmentation. In [16], repeated Gaussian filters are used to accurately segment each beat of a recorder PPG signal and then derive a Signal Quality Index (SQI) is derived based on the temporal consistency of each beat. Another common strategy is to use SQI metrics like perfusion index, zero-crossing rate [17] to analyze the quality of recorded PPG signals. In [18,19], the quasi-periodicity of the PPG signal is quantified in the form of statistical metrics such as skew and kurtosis. Skew, which is a measure of symmetry, is expected to be high in clean PPG segments and low where the segment is contaminated with motion. However, these measures do not capture the PPG waveform variability among subjects, along with the time-varying dynamic properties of the PPG signal. Therefore these techniques have low accuracy in detecting a motion-corrupted segment in real-world scenarios. Time-domain techniques [20] and time–frequency techniques like variable frequency complex demodulation (VFCDM) [21] have also been explored in the past for motion artifact detection in PPG waveforms. The overall idea behind these approaches is that a clean PPG signal's temporal/frequency representation will vastly differ from a motion-contaminated signal. Deep neural networks [22,23] are being used to learn and detect motion artifacts in PPG signal recordings more recently. In [23], the authors propose the use of 1D-CNN architecture to detect motion artifacts in a 5 s signal window. However, deep neural network-based methods generally require a large amount of labeled data for training the network, which might be infeasible.

1.2. Contributions

The techniques discussed above are often ad hoc in their development of detecting motion corrupted signals. An in-depth analysis of the effects of motion artifacts on PPG morphology remains lacking. For instance, most of the prior algorithms have been shown to fail under periodic motion scenarios. Often, motion activities like tapping a finger, shaking, jogging, and running induce periodic motion interference in the PPG signal. In this paper, we propose a more robust technique to deal with all types of motion artifacts. Overall, the contributions of this work are twofold, as described below.

Algorithmic innovation Our proposed approach towards motion detection is based on two assumptions:

1. Clean PPG signal possesses a quasi-periodic structure and can be represented with the help of a signal model. On the other hand, motion signals are challenging to model, and there are currently no known validated signal models that capture the effect of motion on PPG signals. We propose a simple model for motion contamination, where motion signals can be represented as an additive time-localized noise taking non-zero values during the motion event and is zero otherwise.
2. Even if the motion-induced artifacts tend to be periodic due to periodic movements, the shape or morphology of these artifacts differs from the characteristic PPG shape, which can be exploited to detect the presence of motion.

Using these two key insights, we propose a robust algorithm called PPGMotion to detect motion artifacts in PPG signals. The algorithm is derived by describing the clean PPG morphology by a quasi-periodic signal model with prior shape template and modeling motion artifacts as structured sparse outliers to the PPG signal model. We also propose an automatic online method for determining the prior shape template based only on the PPG waveform recorded from the individual subject.

Dataset We use both real and synthetic datasets to evaluate the performance of PPGMotion vs. classical methods. For the synthetic dataset, we propose the use of a generative model to simulate different real-life motion scenarios. The proposed generative model uses two parameters: periodicity factor and Signal-to-Motion Ratio. For real data, we collected pulse-oximeter data from subjects making (1) random finger movements, (2) periodic movements like periodic finger tapping, (3) PPG recordings from Maxim smartwatch with subjects running on a treadmill, and (4) continuous PPG recordings from Maxim smartwatch for a duration of 72 h. Dataset (2) and (3) are expected to introduce periodic motion artifacts in the measured PPG signals, and dataset (4) is supposed to capture real-life motion-contaminated PPG signals.

We demonstrate that while our approach is similar in performance to previous methods when random motion artifacts are introduced, the performance is significantly better in the presence of periodic motion artifacts. We show that for the simulated dataset, the performance of PPGMotion is significantly better than existing work as the contaminated PPG tends to become periodic, with an increase in sensitivity of at least 20% over the state-of-the-art method. For real data, PPGMotion successfully detects the periodic motion artifacts, with a mean sensitivity of 91% and accuracy of 93%, compared to the state-of-the-art method with a mean sensitivity of 77% and accuracy of 90% for the dataset (2). For dataset (1), PPGMotion achieves an accuracy of 94% with a sensitivity of 92%, and for the dataset (3), PPGMotion achieves an accuracy of 90% and sensitivity of 89%, compared to the second-best method with accuracy 81% and sensitivity 75%. We also report average accuracy of 91% on a challenging dataset (4), which validates that PPGMotion can be used reliably to detect motion contamination in real-life scenarios.

2. Problem formulation

The PPG signal associated with the cardiac cycle is quasi-periodic in nature, and it is often modeled by as a non-harmonic waveform [24] that is a combination of amplitude modulated and frequency modulated signals. Thus, over the analysis window, we model the PPG signal, *without* motion artifacts, as

$$y(t) = a(t)s(\theta(t)) + n(t), \tag{1}$$

where $y(t)$ is the observed PPG signal, $a(t)$ is the amplitude envelope, s represents the PPG shape that is 2π-periodic. The pulse shape is given by $s(\theta(t))$ where $\theta(t)$ ranges from 0 to 2π. Henceforth, we will use s to denote a pulse shape, which refers to one period of the base signal $s(t)$. The term $n(t)$ is the sensor noise. Finally, we assume that the pulse shape is constant within the analysis window.

The instantaneous phase $\theta(t)$ of a signal is given by

$$\theta(t) = 2\pi \int_0^t f_{hr}(t)dt, \tag{2}$$

where f_{hr} is the instantaneous frequency that varies according to the heart rate variability. We also assume that the instantaneous phase is a

monotonically increasing function such that $\theta'(t) > 0 \forall t \in \mathbb{R}$.

Since s is a periodic function, it can be represented as a Fourier series and is assumed to be K-bandlimited since the shape is a smoothly varying function. We also assume that all the Fourier modes of the defined PPG shape s are dominated by the Fourier coefficient corresponding to the fundamental frequency.

2.1. Constraints on parameters of the signal model

The heart rate generally does not remain constant but fluctuates slowly over time. Normally, the heart rate variability over time is a low-pass signal [25] with the maximum frequency content of 0.5 Hz. To ensure that $a(t)$ and $\theta'(t)$ are slow varying functions or less oscillatory, we take the approach in [26], where a linear space $V(\theta_0, \lambda)$ is constructed consisting of all functions smoother than $\cos(\theta_0)$,

$$V(\theta_0, \lambda) = \text{span}\left\{\cos\left(\frac{k\theta_0}{2L_\theta}\right), \sin\left(\frac{k\theta_0}{2L_\theta}\right)\right\}_{0 \leqslant k \leqslant 2\lambda L_\theta}, \tag{3}$$

where $\lambda < 1/2$ is a parameter to control the smoothness of functions in $V(\theta_0, \lambda)$, θ_0 is the instantaneous phase corresponding to the average heart rate frequency, $L_\theta = (\theta(T) - \theta(0))/2\pi$, and the signal is recorded from $[0, T]$ in time. The amplitude envelope and the instantaneous frequency lies in the constructed linear space $V(\theta_0, \lambda)$, i.e. $a \in V(\theta_0, \lambda)$ and $\theta' \in V(\theta_0, \lambda)$. We also enforce a prior information on the pulse shape denoted by s and we assume that the temporal variation of the pulse shape of a person is small.

2.2. Motion model

Ideally, the best approach is to rely on a physics-inspired/driven model that accurately captures the physical phenomena. However, there are currently no known validated signal models that capture the effect of motion on PPG signal measurements. Thus, we will adopt a different approach and use modeling to achieve the objective of motion identification. In this case, the model's purpose is to assist in accurate identification but not necessarily explanation of the phenomena. With that in mind, we propose to model the observed signal $y(t)$ in presence of motion contamination as,

$$y(t) = a(t)s(\theta(t)) + m(t) + n(t). \tag{4}$$

The term $n(t)$ in (4) is the sensor noise and can be modeled by a Gaussian distribution having a fixed variance. The motion signal is represented by $m(t)$ and may be present in certain time intervals in the recording span.

We note two important properties of the motion signal. First, motion-contaminated PPG signal morphology differs from that of a clean PPG signal. When the motion activity is periodic, the motion signal $m(t)$ tends to be periodic. However, the self-repeating shape in the contaminated signal differs from that of the characteristic shape possessed by a clean PPG segment in the time-normalized axis, as shown in Fig. 1. The motion signal, when present, can, therefore, be considered as an undesired additive signal to the clean PPG signal component.

Second, the motion events are often localized in time, i.e., they occur for part of the duration within a PPG signal recording, as shown in Fig. 2. The motion signal can be therefore modeled as a sparse signal, containing non-zero values in groups during motion contamination and is zero otherwise.

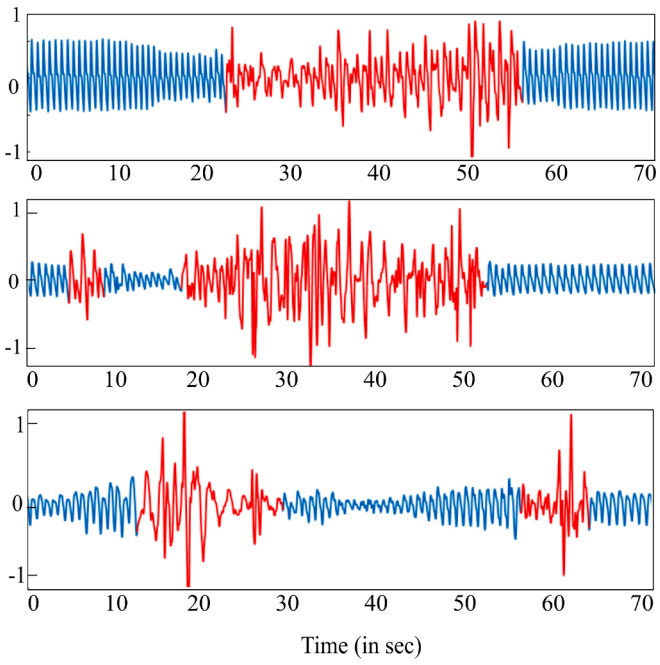

Fig. 2. Time-localized motion contamination. Three instances of motion contaminated PPG signal obtained from a Maxim smart-watch [27]. The motion-contaminated signal (in red) is mostly time-localized in some specific time durations due to the motion activit.ies of the user.

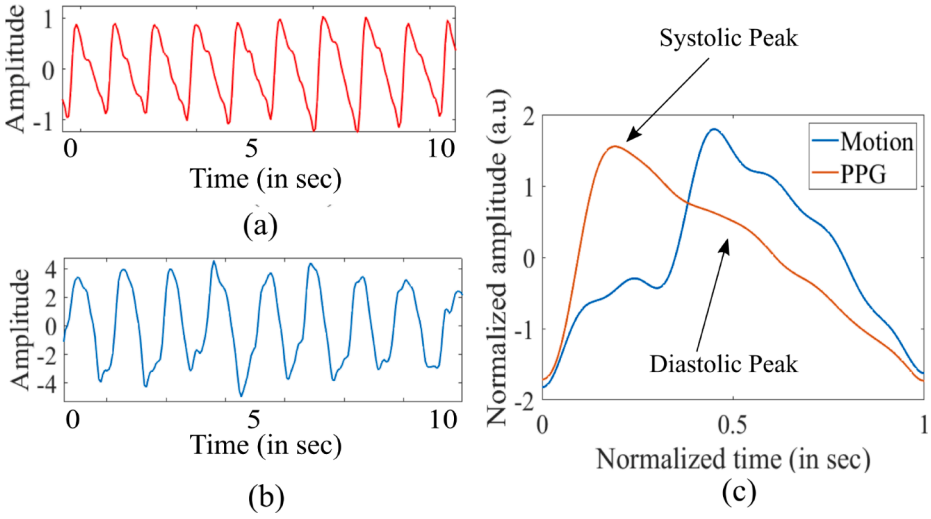

Fig. 1. Shape difference between clean PPG and periodic motion. (a) An example of a clean PPG signal (b) An example of a periodic motion contaminated PPG signal. (c) One period of the clean signal in (a) vs. one period of the contaminated signal in (b), time-normalized to 1 s. The periodic feature of motion contamination makes it difficult to be detected by traditional motion detection algorithms. However, the motion-contaminated segment lacks the distinct features possessed by clean PPG shape, shown in (c), enabling the use of a prior shape template.

2.3. Optimization criterion

First, if a shape template corresponding to a clean PPG segment is known apriori, we can leverage the prior information towards a more accurate detection. In our dataset, we observe a high correlation coefficient between two clean PPG shapes over a short time interval. Therefore, we can constrain the change in PPG shape over a consecutive time window. In other words, if the clean PPG shape is s_0 in a time window T_0, the PPG shape in the next clean time window T_1 should not deviate too much from s_0.

Second, the motion signal is a contiguous sparse signal. To recover sparse models, sparsity-inducing norms have been widely used in the application of compressive sensing [28]. The common formulation is to penalize the l_2 norm criterion by the l_0 norm of the coefficient vector. Additionally, when the signal is assumed to be group-sparse or block-sparse, $l_{2,0}$ norm is commonly used as a regularizer. Since $l_{2,0}$ is non-differentiable, a convex relaxation of $l_{2,0}$ norm, the $l_{2,1}$ norm, is used instead to penalize the l_2 criterion [29]. The use of $l_{2,1}$ norm induces block sparsity or group sparsity [30,31], and has been explored widely with numerous applications in the field of bioinformatics, see e.g. [32]. Using a similar idea, an $l_{2,1}$ penalty can be imposed on the motion signal $m(t)$ to induce contiguous sparse structure on the signal.

Thus, for an observed PPG signal $y(t), t \in [0, T]$, we pose the problem of testing the hypothesis $\mathbf{H_1}$ characterized by (4), against the null hypothesis $\mathbf{H_0}$ characterized by (1), the objective being to determine if the signal $y(t)$ contains a motion contamination in the recording span and localize the motion event if present. The hypotheses are,

$$\begin{aligned}
\mathbf{H_0}: y(t) &= a(t)s(\theta(t)) + n(t) \\
&\text{s.t.} a, \theta \in V(\theta_0, \lambda), ||s - s_0||^2_{\mathscr{F}} \leqslant \epsilon \\
\mathbf{H_1}: y(t) &= a(t)s(\theta(t)) + m(t) + n(t), \\
&\text{s.t.} \begin{cases} a, \theta \in V(\theta_0, \lambda), ||s - s_0||^2_{\mathscr{F}} \leqslant \epsilon, \\ ||m(t)||_{2,1} \leqslant k, \end{cases}
\end{aligned} \tag{5}$$

where s_0 is the priori shape template, and $||.||_{\mathscr{F}}$ denotes the l_2 norm in the Fourier space. The Gaussian noise $n(t)$ is assumed to be zero mean with fixed variance σ. The parameters a, θ, s, m, σ are all unknown and need to be estimated.

The generalized likelihood ratio test (GLRT) is then set up as,

$$r_T = \frac{\max p_{\mathbf{H_1}}(y|s, a, \theta, m, \sigma)}{\max p_{\mathbf{H_0}}(y|s, a, \theta, \sigma)}. \tag{6}$$

The log-likelihood ration η_T, defined as $\eta_T = \frac{\log r_T}{T}$, can be then shown to be given by

$$\begin{aligned}
\eta_T &= -\log \left[\frac{\min\limits_{a,\theta,s,m} ||y(t) - a(t)s(\theta(t)) - m(t)||_2}{\min\limits_{a,\theta,s} ||y(t) - a(t)s(\theta(t))||_2} \right], \\
&\text{s.t.} a, \theta \in V(\theta_0, \lambda), ||s - s_0||^2_{\mathscr{F}} \leqslant \epsilon, ||m(t)||_{2,1} \leqslant k.
\end{aligned} \tag{7}$$

The log-likelihood ratio is then compared to a known threshold λ_{thresh} to select a hypothesis.

We have discrete points from the time series parameters which can be written in terms of vector notations, $\mathbf{y} = [y(1), y(2) \ldots y(N)]$, where N is the total number of samples in one time analysis window. The PPG shape s is represented by its Fourier coefficient vector $\bar{\mathbf{s}}$. Similarly, the other vectorized variables are denoted by bold symbols of their corresponding time-domain notations. The time-domain form of $a(t)s(\theta(t))$ can be rewritten via matrix multiplication as $\mathbf{F_{a,\theta}} \cdot \bar{\mathbf{s}}$, where $\mathbf{F_{a,\theta}}$ is a basis matrix constructed from $\boldsymbol{\theta}$ and $\mathbf{a}$. We refer the readers to [24] for more details. Using the assumptions and the idea of structured sparsity, we rewrite the numerator in (7) as the l_2 norm of the signal residual from the following optimization problem,

$$\begin{aligned}
\widehat{\mathbf{m}} = \; & \text{argmin}_{\mathbf{a},\bar{\mathbf{s}},\boldsymbol{\theta},\mathbf{m}} ||\mathbf{y} - \mathbf{F_{a,\theta}} \cdot \bar{\mathbf{s}} - \mathbf{m}||_2^2 + \lambda_1 ||\bar{\mathbf{s}} - \bar{\mathbf{s}}_0||_2^2 \\
& + \lambda_2 ||\mathbf{m}||_{2,1}, \\
& \text{suchthat}: \mathbf{a}, \boldsymbol{\theta}' \in \mathbf{V}(\boldsymbol{\theta_0}, \lambda), \\
\text{and} \quad & \mathbf{i} = supp(\widehat{\mathbf{m}}),
\end{aligned} \tag{8}$$

where $\boldsymbol{\theta_0}$ is the instantaneous phase corresponding to the average heart rate frequency, $\widehat{\mathbf{m}}$ is an estimation of the motion signal, and *supp* denotes the support of the signal. We define an indicator function $\mathbf{i}$, which denotes where the motion signal is active and is given by the support vector of $\mathbf{m}$. Specifically, when motion signal groups have non-zero values, the indicator function $\mathbf{i}$ is 1 for the corresponding groups and 0 elsewhere. The denominator in (7) is a simple case of (8), and can be posed as a simple ridge regression problem with $\mathbf{m} = \mathbf{0}$. The details of solving for the formulation in (8) is highlighted in the next section.

3. PPGMotion: algorithm for estimation of parameters

There are 4 sets of variables to be estimated in (8), $\boldsymbol{\theta}, \mathbf{a}, \bar{\mathbf{s}}$ and $\mathbf{m}$, and the optimization problem is non-convex. To simplify the optimization process in (8), the problem is broken down into subproblems, using the idea of alternate minimization method [33]. Solving for the parameters follows an iterative procedure where, in an iteration, the loss function is optimized with respect to one variable while the other variables are held fixed. The objective function is optimized over the second parameter with the updated variable kept fixed. This process is repeated until convergence. Under the scheme of alternating minimization process, the optimization subproblem corresponding to estimating $\boldsymbol{\theta}$ is non-convex while the others are convex, which makes the overall problem slightly tractable.

Thus, the proposed PPGMotion algorithm that comprises of following iterative subparts,

1. estimation of the instantaneous phase $\boldsymbol{\theta}$ of the PPG signal. The optimization subproblem is nonlinear and non-convex in and we use a data-driven time frequency analysis [26] to estimate $\boldsymbol{\theta}$.
2. estimation of instantaneous amplitude $\mathbf{a}$, and the pulse shape $\bar{\mathbf{s}}$, which involves solving a ridge-regression problem.
3. estimation of the motion signal $\mathbf{m}$ by solving a group-lasso problem using the estimated PPG signal parameters in the previous step.

Breaking the problem in (8) into subproblems gives rise to the following algorithm for a specific time analysis window,

$$\begin{aligned}
& \text{Initialize } \bar{\mathbf{s}}_0, \mathbf{m}^0 = \mathbf{0}, \\
& \text{for iteration counter} k = 1, 2, .. \\
\mathbf{P1}: \; & \widehat{\bar{\mathbf{s}}}^k, \widehat{\mathbf{a}}^k, \widehat{\boldsymbol{\theta}}^k = \text{argmin}_{\bar{\mathbf{s}},\mathbf{a},\boldsymbol{\theta}} ||\mathbf{y} - \mathbf{F_{a,\theta}} \cdot \bar{\mathbf{s}} - \widehat{\mathbf{m}}^{k-1}||_2^2 \\
& + \lambda_1 ||\bar{\mathbf{s}} - \bar{\mathbf{s}}_0||_2^2, \\
& \text{suchthat}: \; \mathbf{a}, \; \boldsymbol{\theta}' \in \mathbf{V}(\boldsymbol{\theta_0}, \lambda). \\
\mathbf{P2}: \; & \widehat{\mathbf{m}}^k = \text{argmin}_{\mathbf{m}} ||\mathbf{y} - \mathbf{F}_{\widehat{\mathbf{a}}^k, \widehat{\boldsymbol{\theta}}^k} \cdot \widehat{\bar{\mathbf{s}}}^k - \mathbf{m}||_2^2 + \lambda_2 ||\mathbf{m}||_{2,1}. \\
& \text{Repeat until convergence.}
\end{aligned} \tag{9}$$

3.1. Estimation of PPG signal parameters

Solving for the first problem **P1** involves estimating the instantaneous phase $\boldsymbol{\theta}$, the instantaneous amplitude $\mathbf{a}$ and the shape coefficient vector $\bar{\mathbf{s}}$. The optimization problem is tackled in two steps-the instantaneous phase and the amplitude are estimated from the first harmonic of the signal as in [26]. Once $\mathbf{a}$ and $\boldsymbol{\theta}$ are estimated, the estimation of PPG shape $\bar{\mathbf{s}}$ becomes a linear optimization problem, which can be solved easily. Several time–frequency methods like Continuous Wavelet Transform, Hilbert Transform [34], and Synchrosqueezing Transform [35,36,24] are often used to estimate the instantaneous phase from the signal. In our work, we have chosen a more robust, data-driven method

[26] to estimate the instantaneous phase and the amplitude envelope.

Once the parameters **a** and $\boldsymbol{\theta}$ are estimated, the problem **P1** can be framed as a simple ridge regression problem, and the estimate of $\widehat{\bar{\mathbf{s}}}^k$ is given by,

$$\widehat{\bar{\mathbf{s}}}^k = (\mathbf{F}^T_{\underset{\mathbf{a}}{\sim}^k,\boldsymbol{\theta}^k} \mathbf{F}_{\underset{\mathbf{a}}{\sim}^k,\boldsymbol{\theta}^k} + \lambda_1 \mathbf{I})^{-1} [\mathbf{F}^T_{\underset{\mathbf{a}}{\sim}^k,\boldsymbol{\theta}^k} (\mathbf{y} - \widehat{\mathbf{m}}^{k-1}) + \lambda_1 \bar{\mathbf{s}}_0], \tag{10}$$

where $\mathbf{I} \in R^{N \times N}$ is the identity matrix.

One important parameter that we have to decide on is the prior information about the shape, $\bar{\mathbf{s}}_0$. As discussed in the previous section, we note that the PPG signal does not change abruptly across time for a specific subject. Therefore, to ensure smoothness of the pulse shape across time, the estimates of pulse shape in previous time analysis windows are used as a prior shape for the next time window. If for a time window T_w, the estimated shape is denoted as $\widehat{\bar{\mathbf{s}}}_w$, and the priori shape template is denoted by $\bar{\mathbf{s}}_{0w}$, then $\bar{\mathbf{s}}_{0w}$ is calculated as,

$$\bar{\mathbf{s}}_{0w} = \frac{\sum_{l=1}^{w} \tau^{w-l}}{\widehat{\bar{\mathbf{s}}}_{l-1}} \sum_{l=1}^{w} \tau^{w-l}, \tag{11}$$

where τ is the forgetting factor, $0 < \tau \leq 1$, and it places a larger weight on the recent shape estimates. We drop the time window subscript w for the prior shape $\bar{\mathbf{s}}_0$ for notational convenience.

3.2. Estimation of motion signal

Once the parameters in **P1** are estimated, the problem **P2** can be re-written as a group lasso problem for estimating $\widehat{\mathbf{m}}$.

The groups are assumed to be known a priori. In this work, we have assumed the motion event duration is at-least 4 s, therefore the group length for calculating $||\mathbf{m}||_{2,1}$ was assigned to be 4 s, with 50% overlap between the groups. We use the approach in [31] together with ADMM [37] to estimate $\widehat{\mathbf{m}}^k$. An indicator function is used to localize the motion event. According to (12), the indicator function is assigned a value 1 for the groups which form the support for $\widehat{\mathbf{m}}$, and 0 elsewhere,

$$\begin{aligned} &\mathbf{i} = \bigcup_{g \in G} \mathbf{i}_g, \\ &\text{where } \mathbf{i}_g = \mathbf{1} \text{ when } \mathbf{m}_g \neq \mathbf{0}, \\ &\text{and } g \text{ denotes the group.} \end{aligned} \tag{12}$$

Once we estimate all the signal parameters, we plug in the parameter values in (7) for hypothesis testing. We name this algorithm as PPGMotion, and the main steps of the algorithm are highlighted in Fig. 3.

3.3. Implementation details

The tuning parameter λ_2 controls the level of the sparsity of the motion outliers in the PPG signal. Even though the motion events are typically active in a very small duration in a time window, the robustness of our method is not limited to sparse settings, as shown in Fig. 4. In Fig. 4(b), even though motion contamination is present in more than half of the time duration, the support of the estimated motion signal accurately captures the motion contamination duration. However, the accuracy of the estimated PPG signal parameters decreases in non-sparse settings since the algorithm has fewer clean PPG time samples for accurate signal parameter estimation. Typically the value of λ_2 depends on the variance of additive Gaussian noise $n(t)$ in (4) that is generally unknown. On the other hand, the value of the tuning parameter λ_1 depends on the extent of temporal smoothness in the pulse shape. The tuning

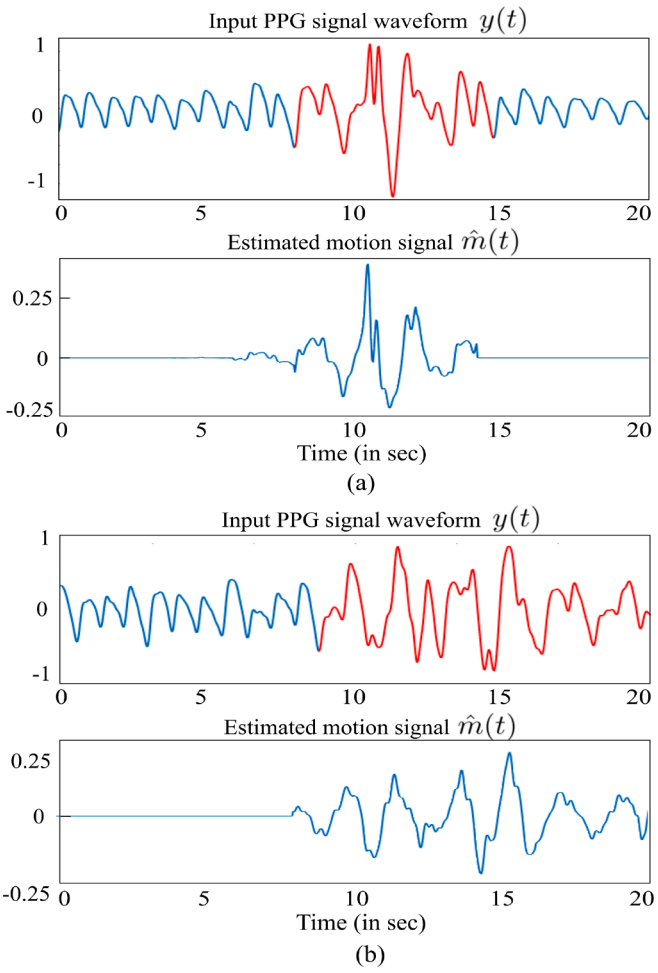

Fig. 4. Intermediate motion signal estimation by PPGMotion. We show two examples of intermediate motion signals estimated by PPGMotion for different duration of motion contaminated PPG signal waveform. The motion contamination is shown in red. The estimated motion signal is zero during clean segments of the input PPG signal due to the group sparsity constraint. The support of the estimated motion signal is not limited to sparse settings only, as evident in (b) for a longer duration motion contamination.

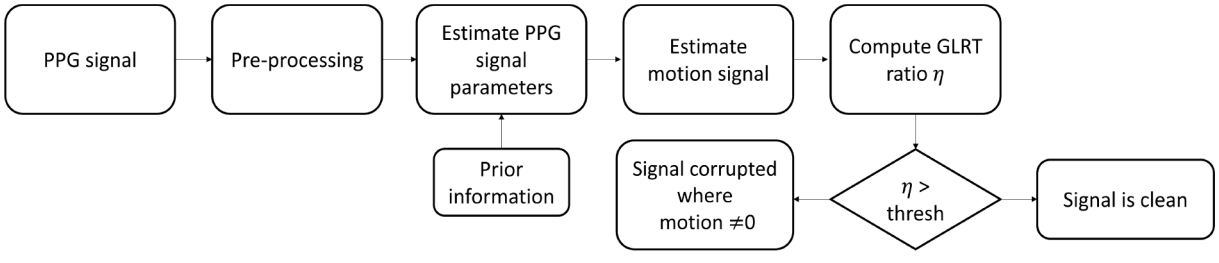

Fig. 3. Block diagram of the PPGMotion algorithm.

parameters λ_1, λ_2 and λ_{thresh} are chosen based on the grid-search method with the objective of maximizing accuracy over a small training dataset.

The PPGMotion algorithm divides the overall PPG signal recording of total time duration T into overlapping time analysis window T_w. In each analysis time window T_w, PPGMotion detects motion corruption in smaller group segments g, where the group segment length can be tuned. For this work, we choose the groups g in a sliding window approach, where each group window corresponds to 4 s duration with 2 s overlap between consecutive groups. More details for choosing the group length are provided in the Discussion section. The choice of time analysis window T_w is mainly based on the assumption that the pulse shape is a periodic function in a small interval. Therefore, the analysis T_w has to be chosen small enough for the assumption to be valid. On the other hand, a too-small value for T_w will result in a high variance in the estimated parameters. For our method, we choose the length of T_w to be 20 s, with an overlap duration of 5 s between two consecutive time windows.

In (3), the value of λ determines the smoothness of the instantaneous frequency and the amplitude function. As mentioned in [26], we chose $\lambda = 0.5$. The cutoff frequency was chosen as 0.5 Hz because it has been reported in several studies [38] that heart rate variability lies within this particular frequency range. In (11), the forgetting factor τ controls the temporal variability of the prior shape template. Based on the data, we chose $\tau = 0.99$.

4. Dataset generation and performance evaluation

In this section, we first mention the prior works we implement to validate the performance of PPGMotion. Next, we describe the process of generating both simulated data as well as real data from participants and compare the results of the PPGMotion algorithm against the prior works on the collected datasets.

4.1. Prior methods for comparison

Since PPGMotion labels a PPG signal segment either clean or corrupt, we compare the performance against some prior methods, which also use binary labels for classification. To compare the PPGMotion algorithm, we implement the idea presented in [21], which uses features from the time-frequency representation of a PPG segment to detect motion corrupted PPG segments. We extract features like projected frequency modulation and HR frequency difference and then train these features with Support Vector Machine (SVM) to distinguish motion contamination and clean counterparts. While the authors in [21] use variable frequency complex demodulation (VFCDM) for feature extraction, we use a readily implemented method, Synchrosqueezing Transform (SST), to extract the time-frequency information. Hence the performance in this work may vary from what is reported before, although we expect the difference in performance to be minimal. We term this approach the SST-SVM method. Secondly, we implement the idea presented in [20], where the features corresponding to morphological variability are considered. We extract features like standard deviation of PPG shape, amplitude, and heart rate variability from a PPG segment window. We use SVM to train the features to differentiate between a clean segment and a motion segment. We term this method TD-SVM. Third, we also implement the idea presented in [39], which uses statistical metrics like skewness and Shanon's entropy to detect motion corruption in PPG signals. We term this method KSE.

4.2. Simulated dataset

Since the experimental dataset provides only limited data points, the synthetic dataset can be used to quantify the performance of our proposed approach on a wide range of motion scenarios.

4.2.1. Generating simulated dataset

With the synthetic dataset, we evaluate the performance PPGMotion by varying two parameters of interest: (i) periodicity and (ii) signal-to-motion ratio.

In any time duration of PPG signal recording in $[0, T]$, the motion artifacts affect some duration $[t_1, t_2]$ in between, where $0 < t_1, t_2 < T$. We represent the motion artifact in a time duration using the following expression,

$$m(t) = \alpha \cdot q(t) + (1-\alpha)g(t), t \in [t_1, t_2], \tag{13}$$

where q is a periodic or a quasi-periodic signal, and g is random aperiodic bandlimited noise. The motion signal is characterized by a periodicity factor α that controls how much periodic component exists in the motion signal, and the overall amplitude is determined by the Signal-to-Motion Ratio (SMR). For $\alpha = 0$, the motion signal is represented by a random noise component, and for α close to 1, the motion signal is represented by a quasi-periodic signal component. Different instances of motion signals are generated using the generative model in (13) with varying periodicity factor α and SMR. The periodic component of the motion signal is generated according to the following equation,

$$q(t) = a_m(t)s_m(\omega t), \tag{14}$$

where $a_m(t)$ is the amplitude envelope, and $s_m(\omega t)$ is a periodic function with fundamental frequency ω.

The amplitude envelope is generated randomly from a Gaussian distribution with mean $\mu = 1$ and variance $\sigma^2 = 10$, and then passed through a low-pass filter with a cutoff frequency of 0.5 Hz. The fundamental frequency ω is chosen uniformly in between 0.5 Hz and 3 Hz because periodic movements like walking or running have a cadence rate of 30 steps per min to 180 steps per min (0.5 Hz – 3 Hz). The function s_m is generated randomly in one period from a Gaussian distribution with mean $\mu = 0$ and variance $\sigma^2 = 1$ and then repeated with a period according to the fundamental frequency ω. To get rid of the high-frequency components, the periodic signal $s_m(\omega t)$ is then passed through a bandpass filter having cutoff frequency 0.5 Hz – 5 Hz, and multiplied with $a_m(t)$ to generate $q(t)$.

Next, we generate the aperiodic random signal component $g(t)$. We collected PPG signals from a pulse oximeter during random arm and finger movements. Analyzing the frequency spectrum of the corrupted PPG signals, we observe that the frequency spectrum is not flat but decays with increasing frequency. If we generate $g(t)$ from a Gaussian distribution, the frequency spectrum will be flat. Instead, we use a colored noise, specifically Brown noise, for generating $g(t)$. The power spectral density of Brown noise is proportional to $1/f^2$; hence the magnitude of frequency spectrum decays with increasing frequency.

The generative model is used to simulate different motion signals by varying values of α and SMR. The generated motion signals are then added to a clean PPG signal component in specific time duration. For a clean PPG signal, we use a PPG signal recording of 2 min duration, acquired from a pulse-oximeter on a completely resting finger from one subject in the dataset (1). Some instances of simulated motion contaminated PPG signal in the frequency domain are shown in Fig. 5 for comparison against some real-life motion scenarios. The frequency spectrum of simulated PPG contaminated data is visually similar to the frequency spectrum of actual contaminated data collected from a pulse oximeter, but we do not have any metric to quantify the similarity.

4.2.2. Evaluation on simulated dataset

The sensitivity for detecting motion contamination by PPGMotion on simulated motion data for SMR −10 dB, −5 dB, 0 dB and 5 dB and for varying α value as is reported in Table 1. Varying the α value controls the proportion of periodic motion signals in the simulated PPG signal. In all of the performance evaluations for the simulated dataset, the specificity for all the methods is comparable; hence we highlight sensitivity alone since only the sensitivity of the methods determines the accuracy. We note several interesting observations from Table 1. First, all the methods have better sensitivity for low α value, and the performance deteriorates

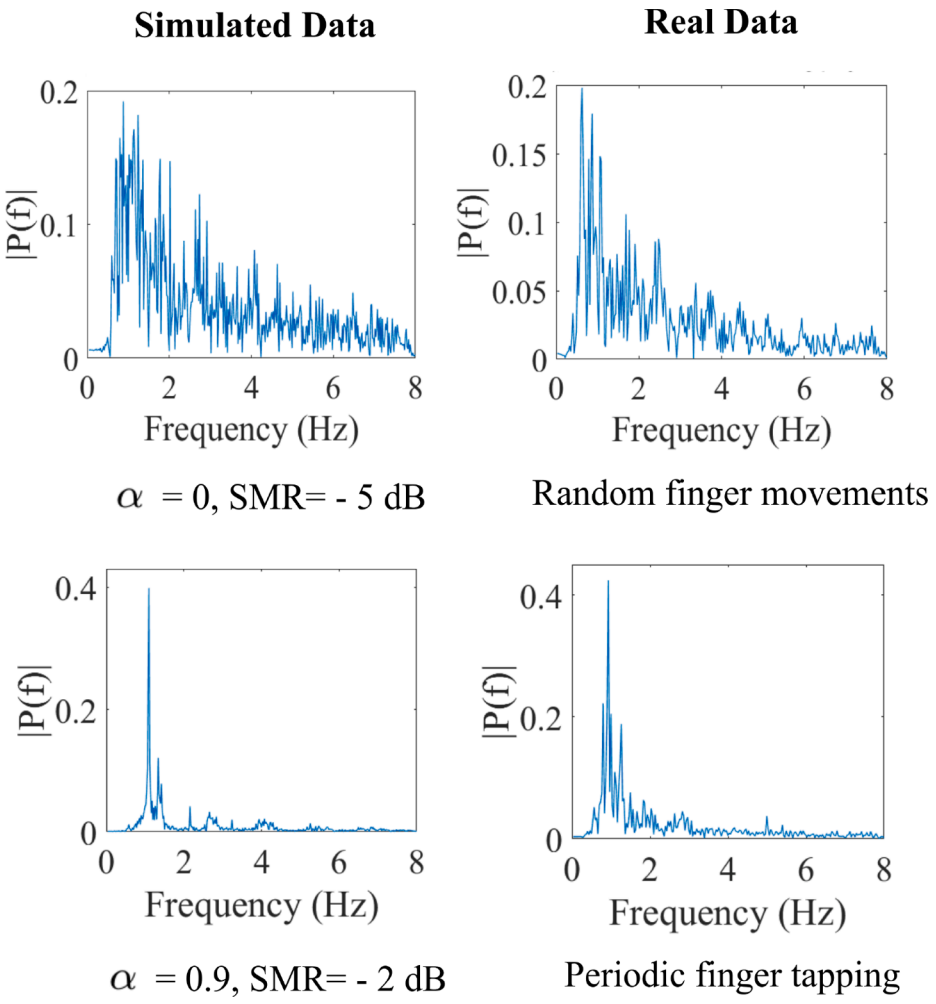

Fig. 5. Synthetic dataset generation for two example cases: the left column shows the frequency spectrum of motion corrupted PPG segments generated synthetically with different α and SMR values as indicated below each plot. The right plot shows examples of real PPG signals acquired from finger pulse-oximeter for different experimental conditions mentioned below each plot. The first row corresponds to a random motion corrupted example, while the second row corresponds to a periodic motion corrupted case. Note that the spectral peaks in the second row are due to periodic motion activity and not due to the heart rate.

as α value increases, which means it is easier to detect random motion contamination than a periodic one. For low α values, the performance of PPGMotion and TDSVM is similar as both the methods are successful in detecting random motion artifacts. However, as seen from the plots in Fig. 6, the sensitivity of TDSVM (second-best method) falls rapidly for increasing α value. The decrease in sensitivity is expected since a high α value denotes the presence of strong periodic motion interference, and the prior methods fail to detect the periodic motion contamination. On the other hand, the decrease in the sensitivity for PPGMotion is more graceful compared to the prior methods. The performance of PPGMotion is around two times better than TDSVM for detecting periodic motion artifacts at a low SMR of -10 dB. Secondly, we observe that the sensitivity for PPGMotion, TDSVM, and SSTSVM mostly increases as we increase SMR for high α values. This increase in sensitivity might be from the fact that when SMR is increasing, the motion contaminated signal has a significant contribution from both quasi-periodic motion signal and the clean PPG signal, due to which the periodicity in the contaminated signal might be lost. Hence the methods perform better in detecting aperiodic motion contamination. In all the cases, PPGMotion has either the same or better performance than all the prior methods.

4.3. Real dataset

The main goal of the experiments reported in this section is to quantify the performance and verify the utility of our proposed PPGMotion algorithm in real-life. We collect data under four sets of experiments that are aimed at capturing different motion scenarios-random, periodic, short, and long duration motion contamination. We evaluate our PPGMotion algorithm on these datasets to detect PPG contamination under real-life motion scenarios.

4.3.1. Experimental data collection methodology

We recruited 17 healthy subjects for the study (8 male, 9 female) in the age group between 24–35 years. All the experiments done in this research were approved by the Rice University Institute Review Board (IRB-FY2018-434, Approval Date: 11/20/2018). We used a BIOPAC pulse oximeter (MP150 module with PPG100C amplifier and TSD200 finger probes; sampling rate of 500 Hz) as well as a Maxim Healthband (sampling rate of 25 Hz) to record the PPG waveforms. We resample the signals acquired from the BIOPAC pulse oximeter to 30 Hz for ease of computation.

4.3.2. Experimental protocol

In the first set of experiments, two probes from the BIOPAC pulse oximeter were connected to the index fingers of the left and right hands. The subjects were asked to stay still initially for 2 min. At the end of 2 min, the subjects were asked to perform random small finger movements for 20 s in one hand while keeping the other hand still. After the movement phase, the subjects were asked to stay still for 30 s. Next, the subjects were asked to perform arm and elbow movements, thus inducing large motion artifacts in the signal. The movement phase lasted for 40 s, followed by 30 s of no activity. The duration of the PPG waveform acquired from each subject was 4 min. We label the dataset acquired from the first experiment as dataset (1).

In the second set of experiments, the subjects were asked to stay still initially for 2 min before the movement phase. Next, they were asked to

Table 1
Sensitivity comparison (Mean ± Std) of PPGMotion vs existing methods on simulated dataset.

Signal-to-Motion Ratio	α value	PPGMotion	TDSVM	KSE	SSTSVM
SMR = −10 dB	$\alpha = 0$	**99.92 ± 0.01**	99.92 ± 0.01	47.32 ± 11.80*	95.34 ± 3.91*
	$\alpha = 0.6$	**99.54 ± 0.48**	95.80 ± 2.15*	27.31 ± 8.15*	70.34 ± 14.80*
	$\alpha = 1$	**84.66 ± 7.53**	47.40 ± 8.56*	21.59 ± 10.10*	49.32 ± 24.08*
SMR = −5 dB	$\alpha = 0$	**99.92 ± 0.01**	99.92 ± 0.01	43.99 ± 8.47*	94.67 ± 3.99*
	$\alpha = 0.6$	**99.84 ± 0.21**	96.40 ± 1.82*	25.62 ± 10.45*	79.99 ± 14.01*
	$\alpha = 1$	**85.90 ± 6.78**	45.49 ± 7.83*	18.93 ± 11.31*	48.30 ± 23.48*
SMR = 0 dB	$\alpha = 0$	**99.91 ± 0.01**	99.92 ± 0.01	42.03 ± 5.61*	95.66 ± 3.11*
	$\alpha = 0.6$	**99.53 ± 0.67**	97.00 ± 1.81*	18.06 ± 8.30*	81.33 ± 11.32*
	$\alpha = 1$	**88.22 ± 6.41**	58.10 ± 8.20*	8.68 ± 11.25*	67.64 ± 19.65*
SMR = 5 dB	$\alpha = 0$	**99.90 ± 0.01**	99.77 ± 0.51	20.37 ± 9.54*	93.37 ± 8.51*
	$\alpha = 0.6$	**99.45 ± 0.78**	97.87 ± 1.71*	11.02 ± 8.62*	83.37 ± 10.54*
	$\alpha = 1$	**94.83 ± 3.54**	75.94 ± 6.50*	10.02 ± 12.23*	77.33 ± 16.26*

(*) indicates statistically significant difference ($p < 0.05$) between PPGMotion and other works.

tap fingers from one hand on a table periodically. Tapping fingers on the table is expected to introduce periodic motion contamination in the recorded PPG signals. The duration of motion activity was 30 s, followed by 30 s of no activity. The duration of PPG waveform acquired from each subject was 3 min. We label the dataset recorded from the second experiment as dataset (2).

In the third experiment, we used a Maxim Health band to record PPG waveform from the wrists of subjects while they were running on a treadmill. The subjects were asked to run for 2 min with a speed of 1, 3, 5 mph with a 2 min resting interval between the activity durations. The duration of PPG signals acquired from each subject was 14 min. We discard data from 3 subjects because the whole duration of the PPG waveform was contaminated with noise and artifacts. We label the dataset from the third experiment as dataset (3).

For the fourth experiment, we used Maxim smartwatch to record PPG waveform from the wrist of 5 subjects. The subjects were asked to wear the smartwatch and continue with their daily activities. The subjects wore the watch continuously for 72 h with intermittent periods of charging in between. This dataset reveals that motion contamination is present in an average of 39% of the total recording time duration.

We use PPG signal measurements from 5 subjects to build a small dataset on which the PPGMotion, and the algorithms based on prior works, are trained. For each algorithm, we obtain two sets of models after training- i) finger model, where the algorithms are trained on pulse-oximeter datasets (1), (2) and, ii) wrist model, where the algorithms are trained on smartwatch dataset (3). The trained models are then validated on respective datasets acquired from the remaining 12 subjects.

4.3.3. Data annotation

We use binary labeling for this work, i.e., we label a PPG segment either clean or corrupted. For datasets (1), (2), and (3), we note the exact start and end time of activity of subjects. Based on the start and end time, we label the entire PPG segment within the activity time duration as a motion corrupted segment. For real dataset (4), the data was recorded in an uncontrolled setting, with no knowledge of activity times, and the absence of any clean reference signal prevented us from using an automated tool for labeling motion contamination. Hence, we resort to visual inspection to label the dataset. An annotator looked at each pulse beat from the PPG signal recordings and labeled them either clean or motion-corrupt. After the labeling process, we repeatedly sample segments of 5 s duration from the entire PPG signal recording, and the segment was shown to a separate inspector for independent labels validation. The random sampling covers approximately 50% (around 35 h) of the whole PPG signal duration. There was a high degree of agreement between the two data labels, with the average Cohen's kappa coefficient being 0.94 between two inspectors.

4.3.4. Evaluation on experimental dataset

In Fig. 7 we show two examples of motion detection for each random motion corrupted PPG segment (left column) from dataset (1) and periodic motion artifact (right column) from the dataset (2), respectively. In the case of random motion corruption, we observe that PPGMotion performs slightly better than the TDSVM method. On the other hand, PPGMotion performs significantly better than the TDSVM method in the case of periodic motion contamination. We quantify the performance of the PPGMotion algorithm against the three existing methods, namely TDSVM, SSTSVM, and KSE for dataset (1), (2), and (3) in Table 2. PPGMotion has higher accuracy in detecting motion artifacts than all existing methods for all the datasets. For the random motion dataset (1), the improvement over the second-best algorithm (TDSVM) is nominal-there is only 2% increase in accuracy and 1% increase in sensitivity. While on the other hand, there is a 15% increase in sensitivity over the TDSVM algorithm for periodic motion dataset (2), and around 3% increase inaccuracy. Similarly, for dataset (3), PPGMotion achieves approximately 9% increase in accuracy and around 25% increase in sensitivity over the TDSVM method. The area under the curve (AUC) for PPGMotion are 0.94, 0.93, and 0.91 for datasets (1), (2), and (3), and is significantly higher than the existing techniques. For the dataset (4), the average accuracy of PPGMotion for dataset (4) is 91.06% as compared to 88.28% achieved by TDSVM. Overall, we observe that PPGMotion performs better in all our datasets.

5. Discussion

PPG signal shape variaion The robustness of the PPGMotion algorithm lies in the assumption that even if the motion artifact tends to be periodic, the shape of the motion corrupted segment is different from the characteristic shape possessed by a clean PPG signal. From our experimental datasets (2) and (3), we estimate the shape from clean PPG segments and a short segment of periodic motion contamination. To quantify the difference in the two estimated shapes, we calculate two metrics; the Normalized Root Mean Squared Error (NRMSE) and the cross-correlation coefficient between the two sets of shapes- i) clean vs. clean (CC) and ii) clean vs. motion (CM). For computing clean vs. clean error metrics, two clean PPG segments before and after motion activity for the same subject are chosen. The NRMSE values for CC are much lower than CM, and vice versa for the correlation coefficient, as shown in Fig. 9, with each metric being significantly different between CC and CM for both datasets (2) and (3). High NRMSE between clean and motion

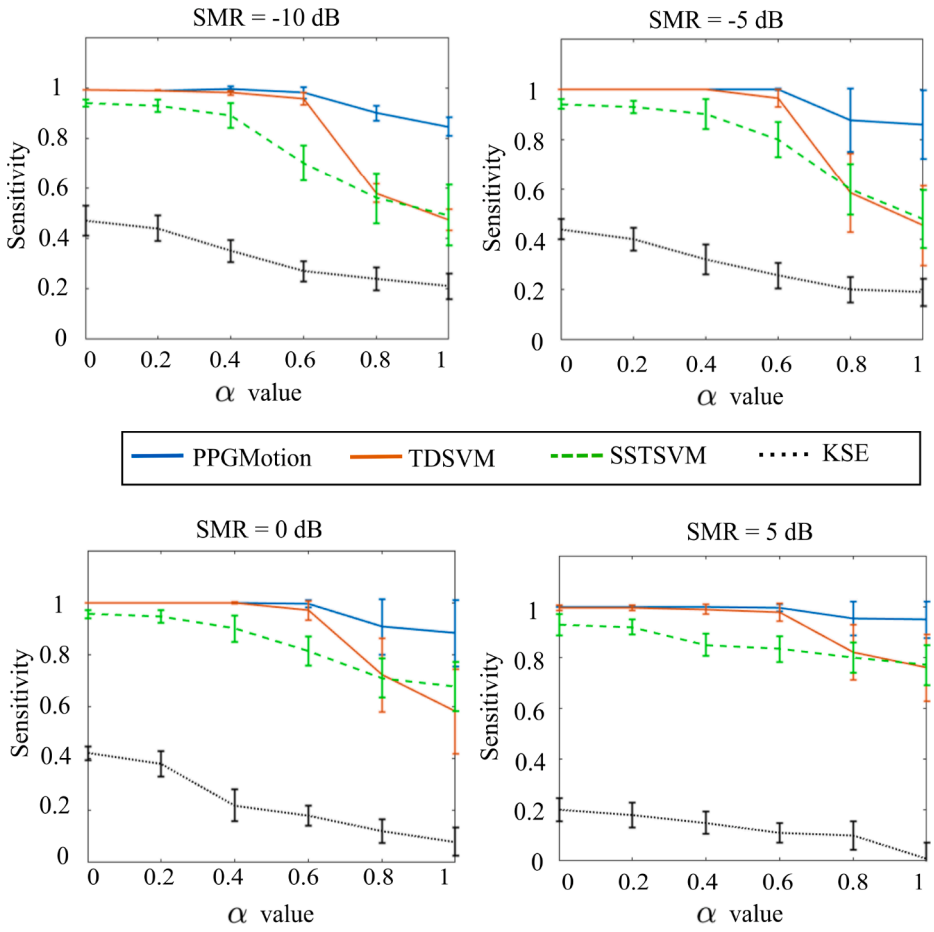

Fig. 6. Sensitivity comparison between PPGMotion and TDSVM. Evaluation of PPGMotion vs TDSVM on simulated data for varying α and SMR = −10 dB, −5 dB, 0 dB and 5 dB. The performance of PPGMotion falls gracefully with increasing α value or periodicity of motion contamination as compared to the sharp decline in performance of TDSVM.

shapes demonstrates that the periodic motion-contaminated PPG shape is significantly different from the clean PPG shape in our datasets.

Motion segment length g We evaluate the influence of motion segment length (size of the group g in 12) on its performance. We take various segment lengths of 2, 4, 6 and 8 s and report the accuracy of PPGMotion on dataset (1), as shown in Table 3. We set the segment size to be 4 s in the PPGMotion algorithm based on the highest accuracy.

Analysis window T_w Choice of larger analysis window T_w will affect any real-time computations like wearable device applications. However, our method doesn't exactly need a PPG waveform for a long duration window. With shorter time analysis windows, the variance of the estimated signal parameters, i.e., heart rate and PPG signal shape, will be high. However, our method should perform the same as long as these parameters are well-constrained with appropriate apriori information (using better initial guesses based on temporal variation of signal parameters). To test this hypothesis, we evaluate our method for various T_w duration for the dataset (1) and (2), as reported in Table 4. We observe that although the accuracy decreases slightly with smaller T_w, the performance of our method is still better than existing methods for all the choices of T_w considered.

PPGMotion as signal filtering In applications that require temporal PPG waveform features such as heart rate variability, our PPGMotion detection algorithm can be extended for PPG signal filtering. The quality of signal filtering, however, depends on the robustness of the heart rate estimate which is used as an initial guess in the PPGMotion algorithm. With a robust heart rate estimator such as TROIKA [10], we can use PPGMotion to estimate the motion signal and hence obtain a clean filtered signal by subtracting the motion signal from the motion corrupted PPG signal. A specific example of our filtering process in small motion contamination is demonstrated in Fig. 10. We see an improvement in the quality of the filtered signal obtained from the PPGMotion algorithm, and it closely matches the clean reference signal obtained simultaneously from a pulse-oximeter put on the resting finger. However, the additive signal model that we consider might no longer be valid in complicated motion scenarios. Hence our filtering technique requires further investigation under these complicated scenarios and can be an interesting extension of our work.

Limitations There are two main limitations to our approach. First, our method will fail in cases where the entire recording duration is corrupted with periodic motion activities or the corruption is present right from the starting of the PPG signal acquisition. In scenarios where there aren't any initial clean PPG segments to reliably estimate the clean PPG shape s_0, our method will fail to distinguish between clean PPG segment and periodic motion corruption. Second, we demonstrate our approach on datasets that comprises healthy young subjects. For healthy subjects, the model assumptions like the consistency of PPG signal beats in short intervals are mostly valid. Some clinical conditions, like atrial fibrillation, cause irregular heartbeats, resulting in widely varying heart rates. Typically, the heart-rate variability is high in people with atrial fibrillation [40], which can be effectively captured by the clean PPG signal model we use in this work. We show one instance of PPG signal waveform from a subject with atrial fibrillation, in Fig. 8, along with the instantaneous frequency estimated in our algorithm and the clean PPG model fitted waveform. The inter-beat interval increases in the presence of a skipped beat, and this is captured effectively by the sudden dip in the estimated instantaneous frequency from the clean PPG signal model.

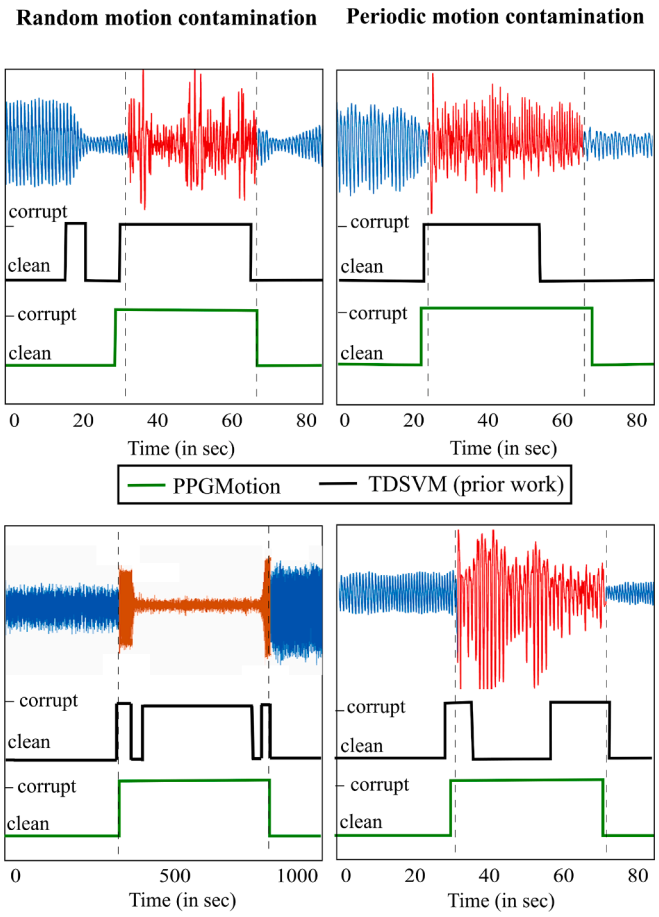

Fig. 7. Performance comparison of PPGMotion against TDSVM for detecting motion contamination: random motion contaminated PPG signal waveform (left column) and periodic motion contaminated PPG signal (right column). For ground-truth labels, the clean segment is plotted in blue and the motion contaminated segment is plotted in red on the signal waveforms. Both TDSVM and PPGMotion perform similarly for detecting random motion contamination, whereas PPGMotion perform clearly outperforms TDSVM in detecting periodic motion contamination.

The estimated PPG shape is unaffected even in the presence of skipped beats. However, detailed analysis needs to be done with more data to draw further conclusions about the performance of PPGMotion to detect motion contamination in clinical settings.

6. Conclusion

We propose a novel algorithm, PPGMotion, for detecting motion artifacts in PPG signals. We also validate the PPGMotion algorithm against other motion-detecting algorithms for different scenarios of

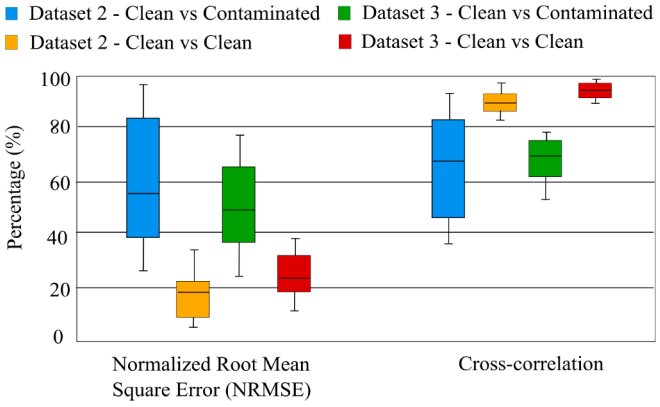

Fig. 9. Shape difference between clean and motion contaminated PPG in our datasets. Normalized root mean square error between clean and motion contaminated shape is larger compared to two clean segments. Similarly normalized cross correlation coefficient for clean and contaminated PPG shape is significantly lower than clean vs clean segments.

Table 3
PPGMotion performance vs length of motion segments

Metric	2 s	4 s	6 s	8 s
Accuracy	91.91 ± 5.10	**94.35 ± 2.67**	93.49 ± 2.81	91.14 ± 4.61
Sensitivity	79.14 ± 8.16	92.25 ± 4.57	**93.00 ± 4.02**	91.52 ± 7.31
Specificity	**95.49 ± 3.71**	94.13 ± 3.40	93.31 ± 4.27	90.75 ± 5.94

Table 4
PPGMotion performance vs time analysis window length

Dataset	Metric	5 s	10 s	15 s
Dataset (1)	Accuracy	92.67 ± 7.72	92.64 ± 3.63	94.15 ± 2.70
	Sensitivity	91.12 ± 6.46	91.72 ± 8.16	92.04 ± 5.99
	Specificity	93.90 ± 10.21	94.20 ± 2.92	94.96 ± 3.96
Datatset (2)	Accuracy	91.74 ± 5.98	92.05 ± 4.60	92.20 ± 2.83
	Sensitivity	87.15 ± 9.60	88.97 ± 8.41	90.31 ± 7.98
	Specificity	92.78 ± 7.13	93.77 ± 6.30	92.94 ± 3.53

Table 2
Performance Metrics (Mean ± Std) of PPGMotion vs existing methods on real dataset (1), (2), (3) and (4)

Dataset	Metric	PPGMotion	TDSVM	KSE	SSTSVM
Finger random movement dataset (1)	Accuracy	**94.35 ± 2.67**	92.49 ± 3.36	85.80 ± 8.60*	92.77 ± 2.65*
	Sensitivity	**92.25 ± 4.57**	90.87 ± 8.60	52.67 ± 20.10*	89.87 ± 2.60*
	Specificity	**95.17 ± 3.4**	92.91 ± 5.96	93.19 ± 6.99*	94.01 ± 2.90
Finger periodic movement dataset (2)	Accuracy	**93.05 ± 2.96**	90.23 ± 3.10	73.06 ± 17.83*	75.89 ± 3.23*
	Sensitivity	**91.86 ± 6.35**	77.38 ± 16.03*	24.89 ± 33*	53.56 ± 27.14*
	Specificity	94.14 ± 3.23	**96.53 ± 2.10**	95.38 ± 3.65	81.89 ± 4.13*
Wrist Exercise dataset (3)	Accuracy	**90.29 ± 1.53**	80.66 ± 15.96*	60.39 ± 5.16*	81.23 ± 2.31*
	Sensitivity	**89.29 ± 5.87**	65.88 ± 32.68*	33.84 ± 10.10*	74.99 ± 11.29*
	Specificity	91.03 ± 5.07	85.08 ± 18.47*	**94.02 ± 2.25**	83.60 ± 14.16*
Wrist Long duration dataset (4)	Accuracy	**91.06 ± 0.94**	88.28 ± 2.96*	80.88 ± 1.17*	86.77 ± 2.74*
	Sensitivity	**90.32 ± 1.85**	78.62 ± 5.15*	70.26 ± 5.71*	81.84 ± 1.34*
	Specificity	91.94 ± 1.15	**94.68 ± 2.84**	87.53 ± 1.01*	90.03 ± 1.69

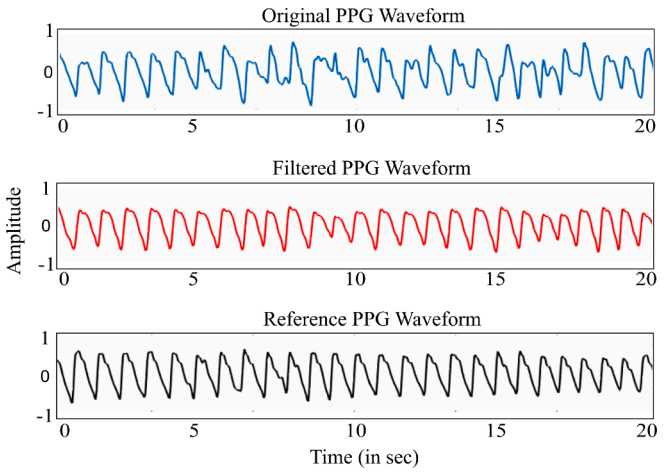

Fig. 10. An example of PPGMotion signal fitlering performance. Motion affected PPG signal (top row), filtered signal from PPGMotion (middle row), and a clean reference signal obtained simultaneously (bottom row). In low motion contamination cases, PPGMotion improves the quality of the PPG signal.

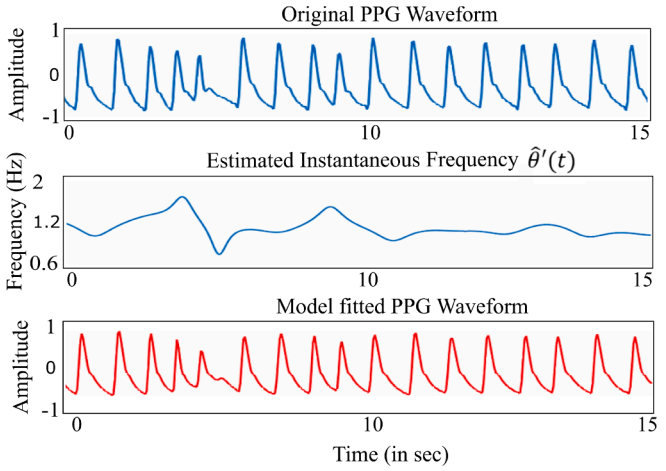

Fig. 8. Clean signal model fitting for a PPG waveform in the presence of a skipped beat. The 5th beat is affected in the original PPG waveform (top row), captured by the sudden dip in estimated instantaneous frequency (middle row). The presence of a slower beat in our model fitted waveform (bottom row) shows that our model can be used in cases of cardiovascular complications.

motion. PPGMotion achieves the same accuracy as that of the state-of-the-art methods when the motion-induced artifacts are random in nature. Whereas on the other hand, in the case of periodic motion-induced artifacts, PPGMotion shows a significant increase in the accuracy of detecting these artifacts. Periodic motion artifacts may arise during daily activities or during cardiopulmonary exercise training [41], and are difficult to handle since traditional algorithms mistake the periodic artifact to be arising from the cardiac activity. We have also demonstrated that PPGMotion can be used as a binary signal quality indicator for continuous PPG-based heart rate monitoring using a commercial device and can be reliably used in real-life applications.

Declaration of Competing Interest

The authors declare that they have no known competing financial interests or personal relationships that could have appeared to influence the work reported in this paper.

Acknowledgement

This work was partially supported by NSF ERC Grant EEC-1648451 (for PATHS-UP ERC).

References

[1] A. Alqaraawi, A. Alwosheel, A. Alasaad, Heart rate variability estimation in photoplethysmography signals using bayesian learning approach, Healthcare Technol. Lett. 3 (2016) 136–142.
[2] C. Park, B. Lee, Real-time estimation of respiratory rate from a photoplethysmogram using an adaptive lattice notch filter, BioMed. Eng. OnLine 13 (1) (2014) 170.
[3] M. Elgendi, On the analysis of fingertip photoplethysmogram signals, Curr. Cardiol. Rev. 8 (2012) 14–25.
[4] K. Pilt, R. Ferenets, K. Meigas, L.-G. Lindberg, K. Temitski, M. Viigimaa, New photoplethysmographic signal analysis algorithm for arterial stiffness estimation, Sci. World J. 2013 (2013) 1–9.
[5] Y. Liang, M. Elgendi, Z. Chen, R. Ward, An optimal filter for short photoplethysmogram signals, Sci. Data 5 (2018).
[6] K. Warren, J. Harvey, K. Chon, Y. Mendelson, Improving pulse rate measurements during random motion using a wearable multichannel reflectance photoplethysmograph, Sensors 16 (2016) 342.
[7] M.R. Ram, K.V. Madhav, E.H. Krishna, N.R. Komalla, K.A. Reddy, On the performance of AS-LMS based adaptive filter for reduction of motion artifacts from PPG signals, in: 2011 IEEE International Instrumentation and Measurement Technology Conference, IEEE, May 2011.
[8] L.B. Wood, H.H. Asada, Low variance adaptive filter for cancelling motion artifact in wearable photoplethysmogram sensor signals, in: 2007 29th Annual International Conference of the IEEE Engineering in Medicine and Biology Society, IEEE, 2007.
[9] B. Roy, R. Gupta, MoDTRAP: Improved heart rate tracking and preprocessing of motion-corrupted photoplethysmographic data for personalized healthcare, Biomed. Signal Process. Control 56 (2020), 101676.
[10] Z. Zhang, Z. Pi, B. Liu, TROIKA: A general framework for heart rate monitoring using wrist-type photoplethysmographic signals during intensive physical exercise, IEEE Trans. Biomed. Eng. 62 (2015) 522–531.
[11] R. Yousefi, M. Nourani, I. Panahi, Adaptive cancellation of motion artifact in wearable biosensors, in: 2012 Annual International Conference of the IEEE Engineering in Medicine and Biology Society, IEEE, 2012.
[12] R. Couceiro, P. Carvalho, R.P. Paiva, J. Henriques, J. Muehlsteff, Detection of motion artifact patterns in photoplethysmographic signals based on time and period domain analysis, Physiol. Meas. 35 (2014) 2369–2388.
[13] J.Y.A. Foo, Comparison of wavelet transformation and adaptive filtering in restoring artefact-induced time-related measurement, Biomed. Signal Process. Control 1 (2006) 93–98.
[14] K. Li, S. Warren, B. Natarajan, Onboard tagging for real-time quality assessment of photoplethysmograms acquired by a wireless reflectance pulse oximeter, IEEE Trans. Biomed. Circuits Syst. 6 (2012) 54–63.
[15] J.A. Sukor, S.J. Redmond, N.H. Lovell, Signal quality measures for pulse oximetry through waveform morphology analysis, Physiol. Meas. 32 (2011) 369–384.
[16] W. Karlen, K. Kobayashi, J.M. Ansermino, G.A. Dumont, Photoplethysmogram signal quality estimation using repeated gaussian filters and cross-correlation, Physiol. Meas. 33 (2012) 1617–1629.
[17] M. Elgendi, Optimal signal quality index for photoplethysmogram signals, Bioengineering 3 (2016) 21.
[18] R. Krishnan, B. Natarajan, S. Warren, Analysis and detection of motion artifact in photoplethysmographic data using higher order statistics, in: 2008 IEEE International Conference on Acoustics, Speech and Signal Processing, IEEE, 2008.
[19] E. Gil, J.M. Vergara, P. Laguna, Detection of decreases in the amplitude fluctuation of pulse photoplethysmography signal as indication of obstructive sleep apnea syndrome in children, Biomed. Signal Process. Control 3 (Jul 2008) 267–277.
[20] J.W. Chong, D.K. Dao, S.M.A. Salehizadeh, D.D. McManus, C.E. Darling, K.H. Chon, Y. Mendelson, Photoplethysmograph signal reconstruction based on a novel hybrid motion artifact detection–reduction approach. part i: Motion and noise artifact detection, Ann. Biomed. Eng. 42 (2014) 2238–2250.
[21] D. Dao, S.M.A. Salehizadeh, Y. Noh, J.W. Chong, C.H. Cho, D. McManus, C.E. Darling, Y. Mendelson, K.H. Chon, A robust motion artifact detection algorithm for accurate detection of heart rates from photoplethysmographic signals using time–frequency spectral features, IEEE J. Biomed. Health Inform. 21 (2017) 1242–1253.
[22] X. Liu, Q. Hu, H. Yuan, C. Yang, Motion artifact detection in PPG signals based on gramian angular field and 2-d-CNN, in: 2020 13th International Congress on Image and Signal Processing, BioMedical Engineering and Informatics (CISP-BMEI), IEEE, Oct 2020.
[23] C.-H. Goh, L.K. Tan, N.H. Lovell, S.-C. Ng, M.P. Tan, E. Lim, Robust PPG motion artifact detection using a 1-d convolution neural network, Comput. Methods Programs Biomed. 196 (Nov 2020), 105596.
[24] H.-T. Wu, H.-K. Wu, C.-L. Wang, Y.-L. Yang, W.-H. Wu, T.-H. Tsai, H.-H. Chang, Modeling the pulse signal by wave-shape function and analyzing by synchrosqueezing transform, PLOS ONE 11 (2016) e0157135.
[25] F. Shaffer, J.P. Ginsberg, An overview of heart rate variability metrics and norms, Front. Public Health 5 (2017).

[26] T.Y. Hou, Z. Shi, Data-driven time-frequency analysis, Appl. Comput. Harmonic Anal. 35 (2013) 284–308.
[27] " https://www.maximintegrated.com/en/products/interface/sensor-interface/max-healthband.html".
[28] M.D. Migliore, A simple introduction to compressed sensing/sparse recovery with applications in antenna measurements, IEEE Antennas Propag. Mag. 56 (Apr 2014) 14–26.
[29] X. Lv, G. Bi, C. Wan, The group lasso for stable recovery of block-sparse signal representations, IEEE Trans. Signal Process. 59 (Apr 2011) 1371–1382.
[30] J. Huang, T. Zhang, The benefit of group sparsity, Ann. Stat. 38 (Aug 2010) 1978–2004.
[31] L. Jacob, G. Obozinski, J.-P. Vert, Group lasso with overlap and graph lasso, in: Proceedings of the 26th Annual International Conference on Machine Learning -, ACM Press, 2009.
[32] F. Nie, H. Huang, X. Cai, C.H.Q. Ding, Efficient and robust feature selection via joint l2, 1-norms minimization, in NIPS, 2010.
[33] A. Gunawardana, W. Byrne, I. Jordan, Convergence theorems for generalized alternating minimization procedures, J. Mach. Learn. Res. (2005) 2049–2073.
[34] Y. Chou, J. Med. Biol. Eng. 34 (4) (2014) 347.
[35] H. Tieng Wu, Instantaneous frequency and wave shape functions (i), Applied and Computational Harmonic Analysis, vol. 35, pp. 181–199, sep 2013.
[36] G. Thakur, E. Brevdo, N.S. Fučkar, H.-T. Wu, The synchrosqueezing algorithm for time-varying spectral analysis: Robustness properties and new paleoclimate applications, Signal Process. 93 (May 2013) 1079–1094.
[37] S. Boyd, Distributed optimization and statistical learning via the alternating direction method of multipliers, Foundat. Trends Mach. Learn. 3 (1) (2010) 1–122.
[38] J.A.J. Heathers, Everything hertz: methodological issues in short-term frequency-domain HRV, Front. Physiol. 5 (May 2014).
[39] N. Selvaraj, Y. Mendelson, K.H. Shelley, D.G. Silverman, and K.H. Chon, "Statistical approach for the detection of motion/noise artifacts in photoplethysmogram," in 2011 Annual International Conference of the IEEE Engineering in Medicine and Biology Society, IEEE, Aug 2011.
[40] S.K. Bashar, D. Han, S. Hajeb-Mohammadalipour, E. Ding, C. Whitcomb, D.D. McManus, K.H. Chon, Atrial fibrillation detection from wrist photoplethysmography signals using smartwatches, Sci. Rep., vol. 9, Oct 2019.
[41] R.W.C.G.R. Wijshoff, M. Mischi, R.M. Aarts, Reduction of periodic motion artifacts in photoplethysmography, IEEE Trans. Biomed. Eng., vol. 64, pp. 196–207, Jan 2017.